Subscripts
1 inner cylinder
2 outer cylinder
P perturbation
x x-component
r r-component
θ θ-component
∞ condition at infinity.

1. Introduction

The study of buoyancy-induced flow and heat transfer in concentric cylindrical annuli is quite important due to it's numerous applications in energy conservation, energy storage, and energy transmission such as nuclear reactors, thermal storage systems, electric transmission cables and electronic component cooling. In most of the earlier theoretical and experimental studies, a two-dimensional (2-D) model was used, in which convection could be assumed to be only within the transverse plane owing to the infinite length of the annulus. A full 3-D analysis was necessary for an annulus with finite axial length, since the viscous shearing effects at the axial end wall had to be accounted for. Vafai and Ettefagh [1] presented a comprehensive literature survey of 3-D buoyancy-driven flow.

Nishimura et al. [2] presented the results of numerical studies done for the reduction of natural convection heat transfer in a horizontal porous annulus heated at the inner surface. They investigated the effect of azimuthal partitions and found that an increase in the number of partitions resulted in a considerable reduction in the heat transfer rate. For a single partition, its position in the annular gap was found to have a negligible effect on the reduction in the heat transfer rate. Hasnaoui et al. [3] carried out a 2-D numerical investigation to study the effect of buoyancy on the fluid flow and heat transfer characteristics between a horizontal cold surface and an infinite array of open cavities heated from below. The symmetry of the flow field, which existed for the case of unbounded flow above the cavities, was found to be destructible due to the presence of an upper wall. At low Ra, steady symmetric two-cell patterns were observed, which gave way to asymmetric patterns at higher Ra. With further increase in Ra, the flow field was found to be periodic before becoming chaotic at very high Ra.

Kwon et al. [4] did a 2-D numerical and experimental study of buoyancy-induced flow and heat transfer in the annulus between horizontal cylinders with three equally spaced axial spacers and found that the natural convection heat transfer was 3–20% less than that for an annulus without the spacers. The heat transfer rate across the annulus was found to be strongly dependent on the location and the thermal conductivity of the spacers with a reduction in the natural convection heat transfer rate by as much as 20% below that for an unobstructed annulus.

Zhang et al. [5] did an experimental study to investigate the laminar natural convection heat transfer and fluid flow in the horizontal annular region between a cylinder and an inner concentric octagonal heated cylinder. They investigated two cases of the octagonal cylinders: one with a complete surface and the other with horizontal slots on the top and bottom surfaces. The overall heat transfer rate was found to be enhanced by as much as 74% for the slotted case while it was found to be slightly lower than that in a cylindrical annulus for the unslotted octagon. Lai [6] numerically studied the effect of three radial baffle designs, i.e. full baffles, partial inner baffles, and partial outer baffles, on the effectiveness of pipe insulation. The 2-D analysis revealed that the effectiveness of the insulation improved with radial baffles. At high Ra, instability was found to occur in the flow and temperature fields. Partial baffles, were, in general, found to be more effective than full baffles.

However, to the best of the authors knowledge, very few studies concerning the effect of different geometric modifications to the concentric cylindrical annuli have been undertaken. The only other study which addresses the above issue was by Iyer and Vafai [7], in which the effects of a single geometric perturbation on the 3-D buoyancy-driven flow and heat transfer in an annular cavity with impermeable end walls was analyzed. In their work, the general patterns and detailed features of the flow and heat transfer in the annulus were presented. Considerable deviation for the co-axial double helical pattern of the cylindrical annulus without any perturbation was observed in the flow field, and the overall heat transfer rate was found to increase considerably. Their work clarified the effect of some key geometric parameters of a single perturbation, such as, the lengths in the axial and radial directions, the axial position of the perturbation in the annulus and that of the gap-width between the cylinders, and a correlation was developed to characterize the overall heat transfer behavior.

In the present work, the effects of multiple geometric perturbations on buoyancy-driven flow in an annular cavity are analyzed and the flow structures corresponding to these different cases are discussed. It was found that the flow field evolved from the entrainment of flow by the heated vertical portion of the perturbation, and qualitative similarity was seen in that the introduction of each additional perturbation altered the flow field in a regular manner. It was observed that with the introduction of multiple perturbations, the overall heat transfer rate increases substantially.

2. Formulation

2.1. Physical model and assumptions

In the current study, natural convection heat transfer in a horizontal cylindrical annulus with different number

of geometric perturbations on the inner cylinder were investigated. Figure 1 shows the four cases, which included those with one, two, three, and four geometric perturbations on the inner cylinder. In addition to these four cases, additional cases were studied to establish the trend for the effects of multiple geometric perturbations. The axial length of the cylinder is taken as 4.0 and that of each perturbation as 0.2. The perturbations are symmetrically placed on the inner cylinder of the annulus. The flow is expected to be symmetric with respect to the vertical circumferential plane. This point was verified in our computational simulations. The physical model and coordinate system used in the present study can be typified by Fig. 2.

In the analysis, the thermophysical properties of the walls and the fluid are assumed to be independent of temperature except for the density in the momentum equation, where the Boussinesq approximation is invoked. The fluid is assumed to be Newtonian and incompressible and the viscous dissipation in the fluid is neglected.

It should be noted that in this work, Ra is defined on the basis of (R_2-R_1) and not R_2, where R_1 and R_2 are inner, outer cylinder radii, respectively. If the Rayleigh number was based on R_2, it would result in a substantially higher value of Ra [8]. The main objective of this work is to establish the effect of multiple perturbations. As such, the main flow field and heat transfer characteristics

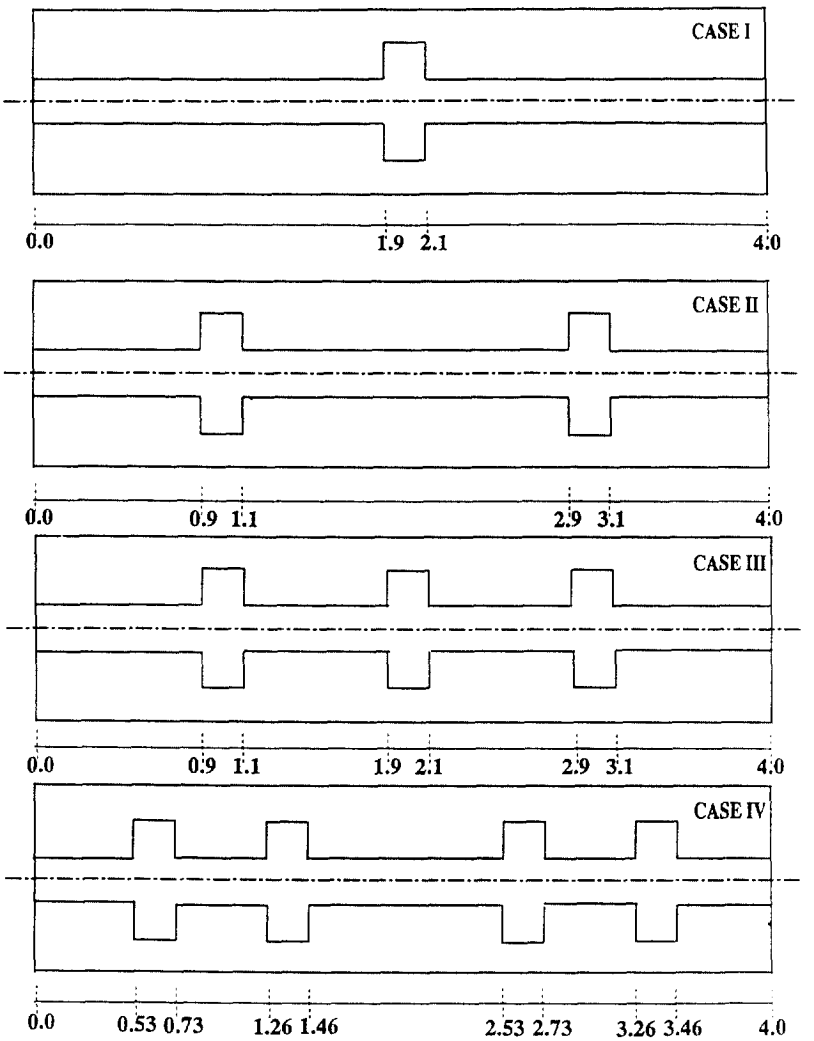

Fig. 1. Schematic representation of cases investigated.

$$T^* = \frac{T - T_\infty}{T_1 - T_\infty}; \quad p^* = \frac{pR_2^2}{\mu\alpha(Ra\,Pr)^{1/2}}. \tag{8}$$

These five equations in terms of the five unknowns, viz. u_x, u_r, u_θ, p and T along with the appropriate boundary conditions fully describe the buoyancy-driven flow in the annulus.

2.3. Boundary conditions

In the current section, for the sake of convenience, the boundary conditions are defined for the annulus with a single perturbation. The boundary conditions for the other cases in the present study are defined in a way which is similar to that presented in this section.

Across the vertical symmetry plane, there is no fluid flow and also no heat transfer. The left and right end walls are assumed to be insulated. The surfaces of the inner cylinder and that of the perturbation are maintained at a constant non-dimensional temperature of unity while that of the outer cylinder is held at a constant non-dimensional temperature of zero. On all rigid and impermeable surfaces, the three components of velocity are zero. The boundary conditions are summarized below:

(1) For the left end wall

$$\text{At } x = 0 \quad \text{and} \quad \frac{R_1}{R_2} \leqslant r \leqslant 1,$$

$$u_x = u_r = u_\theta = 0, \quad \frac{\partial T}{\partial x} = 0. \tag{9}$$

(2) For the right end wall

$$\text{At } x = L_2 \quad \text{and} \quad \frac{R_1}{R_2} \leqslant r \leqslant 1$$

$$u_x = u_r = u_\theta = 0, \quad \frac{\partial T}{\partial x} = 0. \tag{10}$$

(3) For the vertical symmetry plane

$$\theta = 0^\circ \quad \text{and} \quad \theta = 180^\circ$$

$$0 < x \leqslant \frac{L_1}{R_2} \quad \text{and} \quad \frac{R_1}{R_2} \leqslant r \leqslant 1$$

$$\frac{L_1}{R_2} \leqslant x \leqslant \frac{(L_1 + L_P)}{R_2} \quad \text{and} \quad \frac{R_P}{R_2} \leqslant r \leqslant 1$$

$$\frac{(L_1 + L_P)}{R_2} \leqslant x < \frac{L_2}{R_2} \quad \text{and} \quad \frac{R_1}{R_2} \leqslant r \leqslant 1$$

$$u_\theta = 0, \quad \frac{\partial T}{\partial \theta} = 0. \tag{11}$$

(4) For the curved surface of the inner cylinder

$$\text{At } r = \frac{R_1}{R_2} \quad \text{and} \quad 0 < x < \frac{L_1}{R_2}; \quad \frac{(L_1 + L_P)}{R_2} < x < \frac{L_2}{R_2}$$

$$u_x = u_r = u_\theta = 0, \quad T = \frac{T_1 - T_\infty}{T_1 - T_\infty} = 1. \tag{12}$$

(5) For the vertical surfaces of the perturbation

$$\text{At } x = \frac{L_1}{R_2}, \quad \frac{(L_1 + L_P)}{R_2} \quad \text{and} \quad \frac{R_1}{R_2} \leqslant r \leqslant \frac{R_P}{R_2}$$

$$u_x = u_r = u_\theta = 0, \quad T = \frac{T_1 - T_\infty}{T_1 - T_\infty} = 1. \tag{13}$$

(6) For the curved surfaces of the perturbation

$$\text{At } r = \frac{R_P}{R_2} \quad \text{and} \quad \frac{L_1}{R_2} \leqslant x \leqslant \frac{(L_1 + L_P)}{R_2}$$

$$u_x = u_r = u_\theta = 0, \quad T = \frac{T_1 - T_\infty}{T_1 - T_\infty} = 1. \tag{14}$$

(7) For the curved surface of the outer cylinder

$$\text{At } r = \frac{R_2}{R_2} = 1 \quad \text{and} \quad 0 < x < \frac{L_2}{R_2}$$

$$u_x = u_r = u_\theta = 0, \quad T = \frac{T_2 - T_\infty}{T_1 - T_\infty}. \tag{15}$$

2.4. Numerical scheme and computational details

The coupled nonlinear system of governing equations along with the boundary conditions described above were discretized using the Galerkin method of weighted residuals, the details of which can be found in ref. [11]. The segregated solution algorithm, in which the global system matrix is decomposed into smaller submatrices is used to solve the system of equations. The use of this method results in a considerable reduction in storage requirements as compared to that for the global system matrix.

Considerable numerical experimentation was done in order to obtain a grid-independent solution. In the computation, the entire axial length of the annulus was considered, while only half the annulus in the circumferential direction was considered due to the expected symmetry. A number of numerical experiments were also done to verify the circumferential symmetry. For all the cases considered in the current study, satisfactory grid-independent solutions were obtained by using about 50 000 elements.

3. Flow and heat transfer results

3.1. Fluid flow

3.1.1. Background

Natural convection in the annulus between horizontal concentric cylinders of finite axial length has been studied extensively and has revealed the presence of a 2-D crescent shaped vortex. The annulus with a finite axial length necessitated 3-D analysis to account for the viscous shear-

ing effects at the end walls. Vafai and Ettefagh [1], Takata et al. [9], and Ozoe et al. [10] obtained a co-axial double helical pattern in which a given fluid particle introduced at one end of the annulus approached the central region of the annulus drawing a small crescent-shaped vortex, turned around at the mid-axial location and returned towards the end that it started from by drawing a larger crescent-shaped vortex outside the smaller one.

Iyer and Vafai [7] presented the 3-D flow-field in a cylindrical annulus of finite axial length in which a single geometric perturbation was introduced on the inner cylinder. Considerable changes from the co-axial double helical flow pattern were observed in the flow field with the introduction of the geometric perturbation. The essential feature of the flow field involved the entrainment of fluid by the heated vertical surface of the perturbation. This entrained fluid would move towards the axial symmetry plane, where, it would turn around and return towards the end wall. It was found that the bulk of the flow returned towards the end wall through the upper circumferential half of the annulus. Also, as in the case of an annulus without a perturbation, the viscous shearing effects at the end wall produced counterclockwise and clockwise rotating cells in the circumferential symmetry plane region of the left and right end walls, respectively.

3.1.2. Flow field description

In order to understand the nature of the flow field with the introduction of multiple perturbations on the inner cylinder, a systematic approach was adopted. The approach involved careful scrutiny of the velocity vectors at numerous axial planes along the annulus with a view to physically visualize the entire flow field. For brevity, the flow field description is presented only for the first four cases. The flow fields for all the six cases were found to be qualitatively quite similar, and the introduction of each additional perturbation was found to alter the flow field in a regular and recurring manner. Another feature, which is common to all the six cases, is that, most of the interesting and noteworthy aspects of the flow field are found to be concentrated in the vicinity of the upper half of the circumferential symmetry plane. Hence, it was found that the velocity vector field in the circumferential symmetry plane, as shown in Fig. 3, will succinctly capture the essential features of the flow field.

As was the case for the annulus with a single perturbation, the flow field is seen to evolve from the entrainment of flow by the heated vertical portion of the perturbation. For the annulus with two perturbations, the rising fluid from either vertical side of the perturbation meet in the upper portion of the annulus near the circumferential symmetry plane causing a local stagnation zone. However, for the annulus with three perturbations, the above feature is seen prominently only for the centrally located perturbation. For the annulus with four perturbations, no stagnation zones are seen in the immediate vicinity of the perturbations. However, in the region between the two perturbations, the strength of the flow field is seen to be very weak.

A look at the velocity vector plots in the circumferential symmetry plane suggests that the flow field is very strongly three dimensional; hence a 2-D assumption will not suffice at any axial cross-section of the annulus

3.2. Heat transfer

3.2.1. Background

The local Nusselt numbers for the inner and the outer cylinders are given by

$$Nu_1 = \frac{h_1 D_1}{2k} \ln\left(\frac{D_2}{D_1}\right) \quad \text{and} \quad Nu_2 = \frac{h_2 D_2}{2k} \ln\left(\frac{D_2}{D_1}\right) \tag{16}$$

where h_1 and h_2 are the local heat transfer coefficients on the inner and the outer cylinders and are, respectively, given by

$$h_1 = \frac{q_{w1}}{(T_1 - T_2)} \quad \text{and} \quad h_2 = \frac{q_{w2}}{(T_1 - T_2)} \tag{17}$$

where q_{w1} and q_{w2} are the heat fluxes per unit area for the inner and the outer cylinder surfaces, respectively.

These non-dimensional heat fluxes are given by

$$q_w = \frac{\partial T}{\partial n} \tag{18}$$

where n denotes the normal pointing outwards from the surface over which the Nusselt number is to be calculated.

On the curved surface of the perturbation, the Nusselt number is given by

$$Nu_P = \frac{1}{(T_1 - T_2)} \left(\frac{D_P}{2k}\right) \frac{\partial T}{\partial n} \ln\left(\frac{D_2}{D_P}\right) \tag{19}$$

and the average Nusselt number over a surface area is given by

$$\overline{Nu} = \frac{1}{A} \int \frac{\partial T}{\partial n} \mathrm{d}A. \tag{20}$$

3.2.2. Local Nusselt number distribution

Figures 4 and 5 show the local Nusselt number distribution on the inner and outer cylinders, respectively, for four of the cases investigated in the current study. The local Nusselt number is plotted as a function of the circumferential and axial coordinates at a Ra of 10^4 over half the axial length of the annulus due to the observed symmetry. This symmetry condition was confirmed through the computational results. It must be noted that the variations of the local Nusselt number on the inner cylinder for the four cases represent the variations on the unperturbed curved surface of the inner cylinder and the surface of the geometric perturbation. The discussion of the Nusselt number distribution for the different cases has been subdivided into two sections viz., for the inner cylinder and that for the outer cylinder.

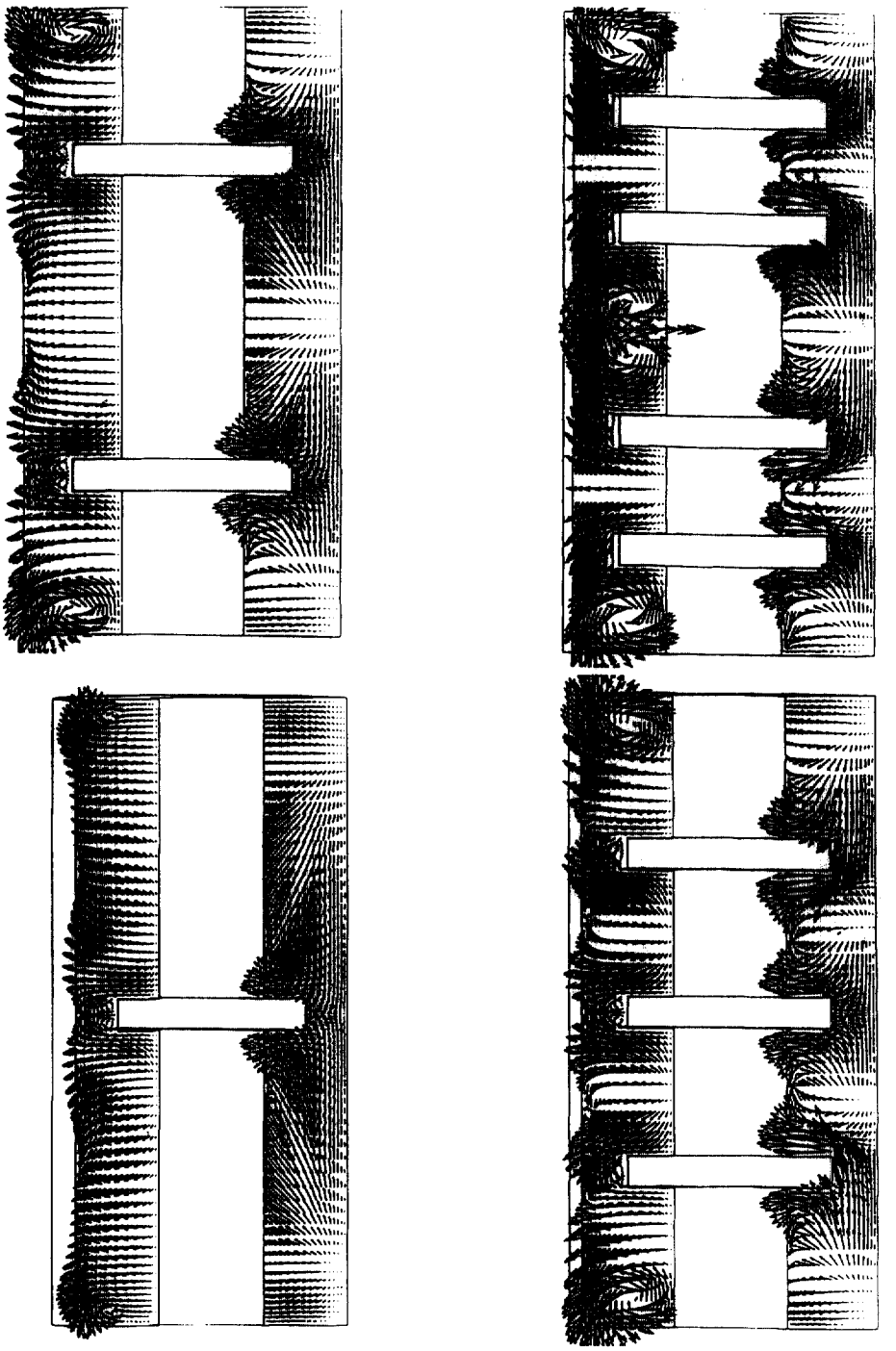

Fig. 3. Velocity vectors in the angular symmetry plane.

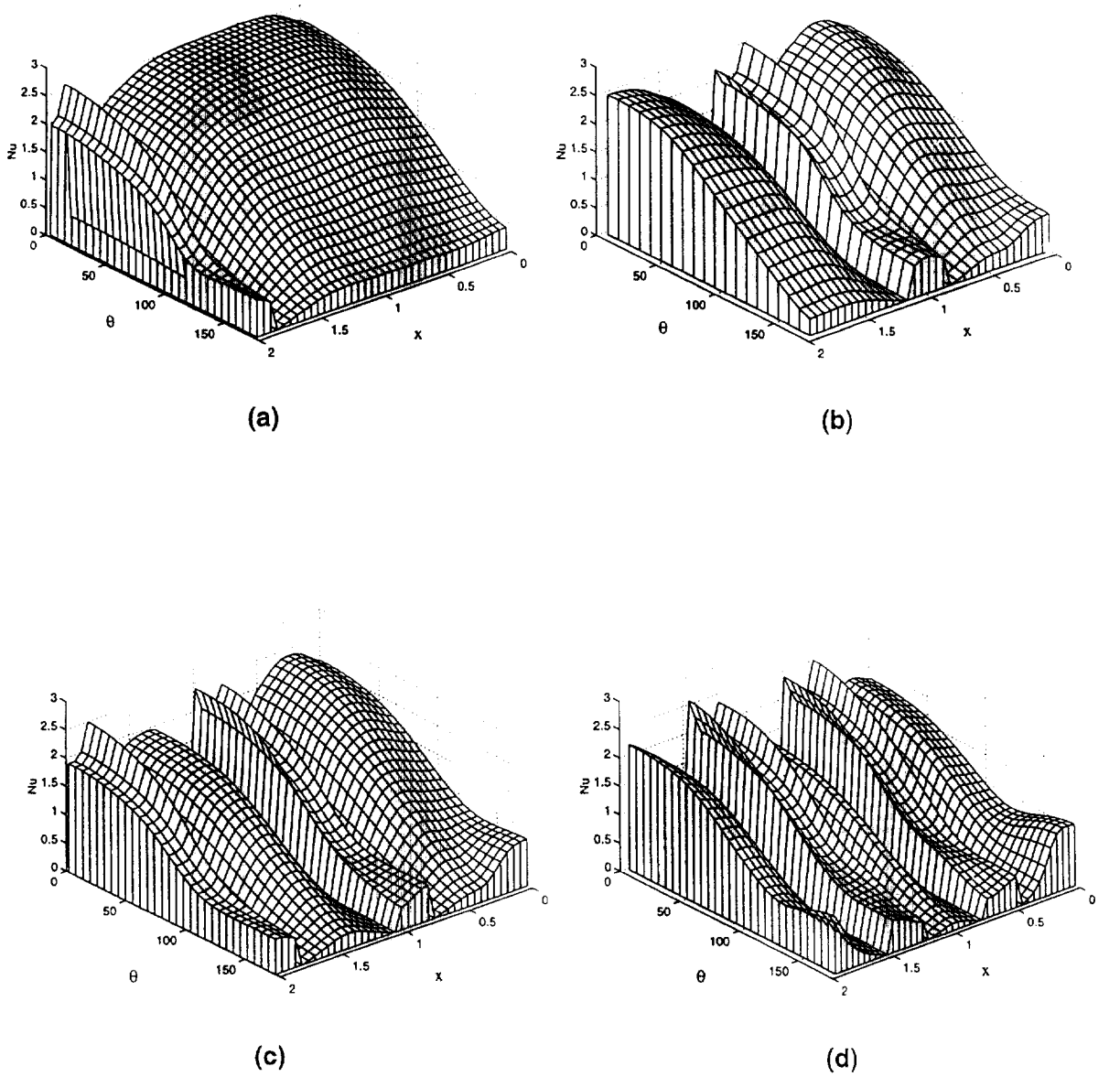

Fig. 4. Local Nusselt number distribution at $Ra = 10^4$ on inner cylinder for annulus with (a) one, (b) two, (c) three, and (d) four geometric perturbations corresponding to cases I–IV of those shown in Fig. 1.

3.3. *Inner cylinder*

It can be seen from Fig. 4 that the local Nusselt number distributions on the inner cylinder are qualitatively similar for the four cases. The Nusselt number increases steadily from a low value in the upper circumferential region to a higher value in the lower circumferential region. A comparison of the local Nusselt number distributions on the inner cylinder for the four different cases reveals that the inclusion of each additional perturbation produces basically the same effect. In the vicinity of the vertical surface of the perturbation, the flow undergoes a reversal after striking the vertical surface of the perturbation causing a significant reduction in the flow velocity in this region, which in turn causes a reduction in the local Nusselt number. In the region above the perturbation, the local Nusselt number was again seen to increase steadily from a lower value in the upper circumferential region to a higher value in the lower circumferential region.

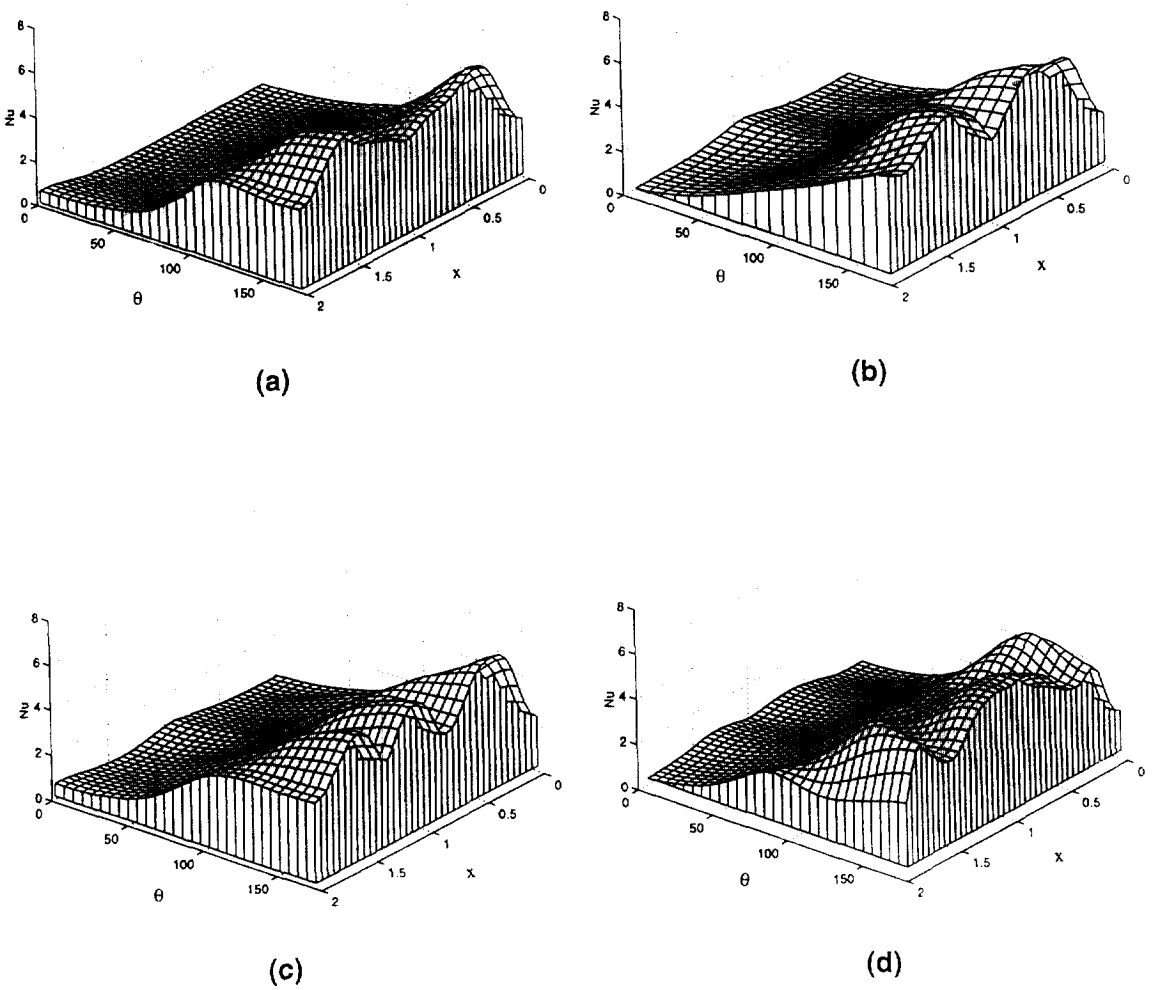

Fig. 5. Local Nusselt number distribution at $Ra = 10^4$ an outer cylinder for annulus with (a) one, (b) two, (c) three, and (d) four geometric perturbations corresponding to cases I–IV of those shown in Fig. 1.

3.4. Outer cylinder

As for the inner cylinder, the local Nusselt number distributions on the outer cylinder for the four cases are also qualitatively similar. As expected, the local Nusselt number increases from the bottom to the top of the annulus due to the impinging flow field near the top of the outer cylinder. A feature common to all the four cases is the crest near the end wall, which is due to the viscous effects of the end wall, and was also observed for the annulus without any geometric perturbation. As was discussed in Iyer and Vafai [7], for the annulus with a single perturbation, a crest is seen in the axial location corresponding to the region near the top of the circumferential symmetry plane, where the rising entrained fluid impinges on the outer cylinder (Fig. 3). The decrease in the local Nusselt number as the axial symmetry plane ($x = 2.0$) is approached can be attributed to the stagnation zone formed above the perturbation in the upper circumferential region of the annulus near the circumferential symmetry plane. Physical explanations on essentially the same lines as above can be provided to explain the crests and troughs seen in the other three cases. In other words, the distributions of the local Nusselt number on the outer cylinder for all the cases considered in the current study can be closely associated to the corresponding flow fields near the circumferential symmetry plane, as depicted in Fig. 3.

3.4.1. Overall heat transfer behavior

In order to assess the influence of the multiple perturbations on the overall heat transfer behavior, the aver-

age Nusselt number characteristics are analyzed. Figure 6 shows the average Nusselt number as a function of Ra for the six cases investigated in the current study. As it can be seen, considerable heat transfer enhancements can be obtained with the inclusion of additional perturbations on the inner cylinder of the annulus. The results can be well correlated by the following equation:

$$\overline{Nu} = 0.71Ra^{0.1}(1+0.12P) \tag{21}$$

where P refers to the number of perturbations on the inner cylinder. The above correlation is valid for $10^3 \leqslant Ra \leqslant 10^4$ and $1 \leqslant P \leqslant 6$. It is evident from Fig. 6 that the rate of increase of the average Nusselt number with the number of perturbations decreases with an increase in the number of perturbations. For a given axial length of the perturbation and the annulus, the increase in the average Nusselt number with the number of perturbations is expected to occur up to a certain limit.

3.5. *Effect of geometric variations*

In a previous work (Iyer and Vafai [7]), the influence of key geometric parameters on the heat transfer performance was thoroughly investigated. The geometric parameters which were considered included the lengths of the perturbation in the axial and radial directions, the axial position of the perturbation in the annulus, and the gap width between the inner and the outer cylinders. It was observed that at any given Rayleigh number, the average Nusselt number increased with an increase in the axial and radial lengths of the perturbation, the effect being more prominent at lower Rayleigh numbers. With an increase in the gap width between the inner and the outer cylinders, the average Nusselt number was seen to increase. These geometric parameters are expected to have approximately a similar influence for the case of multiple perturbations. The results from the previous study (Iyer and Vafai [7]) were combined with those from the current study to yield an approximate correlation, in an attempt to capture the effects of the Rayleigh number, the axial and radial lengths of the perturbation, and also that of the number of perturbations. This approximate correlation is given as

$$\overline{Nu} = 0.33Ra^{0.1}(1+0.78r^*)(1+2.75x^*)(1+0.08P) \tag{22}$$

In the above correlation, r^* is the dimensionless length in the radial direction, and is defined as the ratio of the height of the perturbation to that of the gap width of the annulus. The dimensionless length in the axial direction,

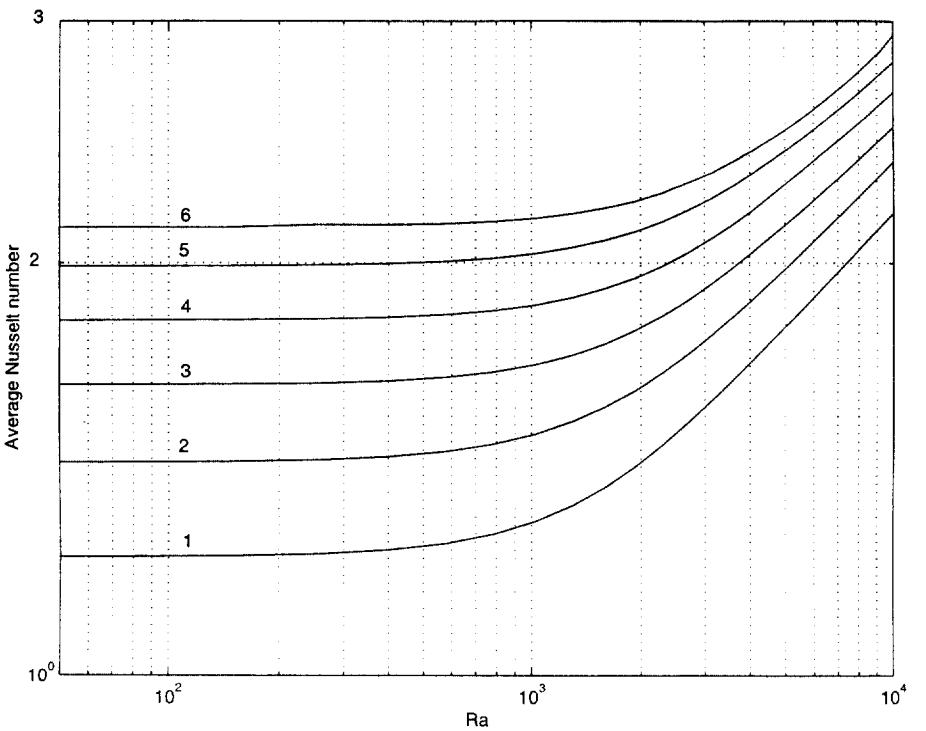

Fig. 6. Average Nusselt number for the six cases.

x^* is defined as the ratio of the axial length of the perturbation to that of the entire annulus.

4. Conclusion

In this work, buoyancy-induced flow and heat transfer in a cylindrical annulus with multiple perturbations on the inner cylinder has been investigated. Detailed analyses of the flow field structures corresponding to these different cases showed that the flow field evolved from the entrainment of flow by the heated vertical portion of the perturbation and qualitative similarity was seen in that the introduction of each additional perturbation altered the flow field in a very regular manner. The heat transfer characteristics were also examined for the different cases and qualitative similarity in the local Nusselt number distributions were observed too. For all the cases considered in the present study, the local Nusselt numbers were found to be closely associated to the corresponding flow fields. Considerable enhancements were seen in the overall heat transfer rate with the introduction of multiple perturbations. The average Nusselt numbers for the different cases could be correlated as $\overline{Nu} = 0.71 Ra^{0.1}(1+0.12P)$, where P refers to the number of perturbations on the inner cylinder.

References

[1] Vafai K, Ettefagh J. An investigation of transient three-dimensional buoyancy-driven flow and heat transfer in a closed horizontal annulus. Int J Heat Mass Transfer 1991;34:2555–70.

[2] Nishimura T, Kunitsugu K, Itoh T. Natural convection suppression by azimuthal partitions in a horizontal porous annulus. Numerical Heat Transfer, Part A 1996;29:65–81.

[3] Hasnaoui M, Bilgen E, Vasseur P. Natural convection above an array of open cavities heated from below. Numerical Heat Transfer, Part A 1990;18:463–82.

[4] Kwon SS, Kuehn TH, Lee TS. Natural convection in the annulus between horizontal circular cylinders with three axial spacers. Journal of Heat Transfer 1982;104:118–24.

[5] Zhang HL, Wu QJ, Tao WQ. Experimental study of natural convection heat transfer between a cylindrical envelope and an internal concentric heated octagonal cylinder with or without slots. Journal of Heat Transfer 1991;113:116–21.

[6] Lai FC. Improving effectiveness of pipe insulation by using radial baffles to suppress natural convection. Int J Heat Mass Transfer 1993;36:899–906.

[7] Iyer SV, Vafai K. Effects of geometric perturbation on buoyancy induced flow and heat transfer in a cylindrical annulus. Int J Heat Mass Transfer 1997;40:2901–11.

[8] Vafai K, Ettefagh J. Axial transport on natural convection inside of an open-ended annulus. ASME Journal of Heat Transfer 1991;113:627–34.

[9] Takata Y, Iwashige K, Fukuda K, Hasegawa H. Three-dimensional natural convection in an inclined cylindrical annulus. Int J Heat Mass Transfer 1984;27:745–54.

[10] Ozoe H, Shibata T, Churchill SW. Natural convection in an inclined circular cylindrical annulus heated and cooled on its end plates. Int J Heat Mass Transfer 1981;24:727–37.

[11] FIDAP Theory Manual. Evanston, IL: Fluid Dynamics International, 1993.